A Molecular Dynamics Study of the Thermodynamic Properties of Calcium Apatites. 1. Hexagonal Phases

Fernando J. A. L. Cruz, José N. Canongia Lopes, and Jorge C. G. Calado*

Centro de Química Estrutural, Complexo Interdisciplinar, Instituto Superior Técnico, 1049-001 Lisboa, Portugal

Manuel E. Minas da Piedade

Departamento de Química e Bioquímica, Faculdade de Ciências, Universidade de Lisboa, 1649-016 Lisboa, Portugal

Received: August 3, 2005; In Final Form: September 30, 2005

Structural and thermodynamic properties of crystal hexagonal calcium apatites, $Ca_{10}(PO_4)_6(X)_2$ (X = OH, F, Cl, Br), were investigated using an all-atom Born−Huggins−Mayer potential by a molecular dynamics technique. The accuracy of the model at room temperature and atmospheric pressure was checked against crystal structural data, with maximum deviations of ca. 4% for the haloapatites and 8% for hydroxyapatite. The standard molar lattice enthalpy, $\Delta_{lat}H_{298}°$, of the apatites was calculated and compared with previously published experimental results, the agreement being better than 2%. The molar heat capacity at constant pressure, $C_{p,m}$, in the range 298−1298 K, was estimated from the plot of the molar enthalpy of the crystal as a function of temperature, $H_m = (H_{m,298} - 298C_{p,m}) + C_{p,m}T$, yielding $C_{p,m} = 694 \pm 68$ J·mol^{-1}·K^{-1}, $C_{p,m} = 646 \pm 26$ J·mol^{-1}·K^{-1}, $C_{p,m} = 530 \pm 34$ J·mol^{-1}·K^{-1}, and $C_{p,m} = 811 \pm 42$ J·mol^{-1}·K^{-1} for hydroxy-, fluor-, chlor-, and bromapatite, respectively. High-pressure simulation runs, in the range 0.5−75 kbar, were performed in order to estimate the isothermal compressibility coefficient, κ_T, of those compounds. The deformation of the compressed solids is always elastically anisotropic, with BrAp exhibiting a markedly different behavior from those displayed by HOAp and ClAp. High-pressure $p-V$ data were fitted to the Parsafar−Mason equation of state with an accuracy better than 1%.

1. Introduction

Apatites are a class of compounds of general formula $M_{10}(PO_4)_6X_2$, where M is a divalent metal cation (primarily Ca^{2+}, Sr^{2+}, Ba^{2+}, Cd^{2+}, or Pb^{2+}), and X is a monovalent anion (OH^-, F^-, Cl^-, and Br^-). The calcium derivatives are by far the most abundant, and they constitute one of the principal host phases for condensed phosphorus and halogens in the solar system,[1−4] at temperatures below ca. 700 K. Hydroxyapatite (HOAp) is a major constituent of mammalian bone and teeth enamel, where it occurs as a nonstoichiometric, amorphous, and carbonated form, but it is also very important as a biomaterial for medical implants.[5−8] Fluorapatite (FAp) is the most commonly occurring calcium apatite, whereas both pure chlorapatite (ClAp) and bromapatite (BrAp) do not occur naturally on Earth, although they can be found in some astral bodies such as meteorites.[3] The structure of the apatites is basically a crystal lattice composed of tetrahedral phosphate anions and calcium cations, with the hydroxyl and halide ions lying on the crystallographic *c*-axis perpendicular to the planes defined by three calcium ions. The stacking of these planes results in a series of parallel hexagonal pipes where the substituents are located (Figure 1a). While the fluoride ions are exactly located on the triangle centers, the hydroxyl, chloride, and bromide ions are increasingly shifted toward a position above those triangles (Figure 1b), resulting in an overall hexagonal symmetry ($P6_3/m$).

As far as the authors are aware, only hydroxy- and fluorapatite have been the subject of molecular dynamics studies. On the basis of structural data and electronic structure calculations, Mkhonto[9] and de Leeuw[10] have proposed potential energy models for FAp and HOAp, respectively. Hauptmann et al.[11] studied both monoclinic hydroxyapatite and hexagonal fluorapatite and fitted experimental data and quantum-chemical calculation results to describe the solids using a Born−Huggins−Mayer type potential. Meis et al.[12] developed a similar potential energy function for fluorapatite, modeling the phosphate tetrahedra with a three-body short-range harmonic potential.

The purpose of this work is to calculate the cohesive energy of the apatites and study the evolution of their structures under high-temperature or high-pressure conditions by assuming the Born model of ionic solids[13] and using a molecular dynamics (MD) technique to perform the relevant calculations. Simulation runs at room temperature ($T = 298$ K) and atmospheric pressure ($p = 1$ bar) were used to calculate the standard molar lattice enthalpy of the different crystals; high-temperature simulations in the range 298 K < T < 1298 K were used to estimate their heat capacity at constant pressure; and high-pressure runs in the range 0.5 kbar < p < 75 kbar were performed to yield the corresponding isothermal compressibility values.

2. Theoretical Methods

Force Field Model. All apatite molecules in this work were modeled by an all-atom force-field based on a four-parameter

* To whom correspondence may be addressed. E-mail: jcalado@ist.utl.pt.

10.1021/jp054304p CCC: $30.25
Published on Web 12/02/2005

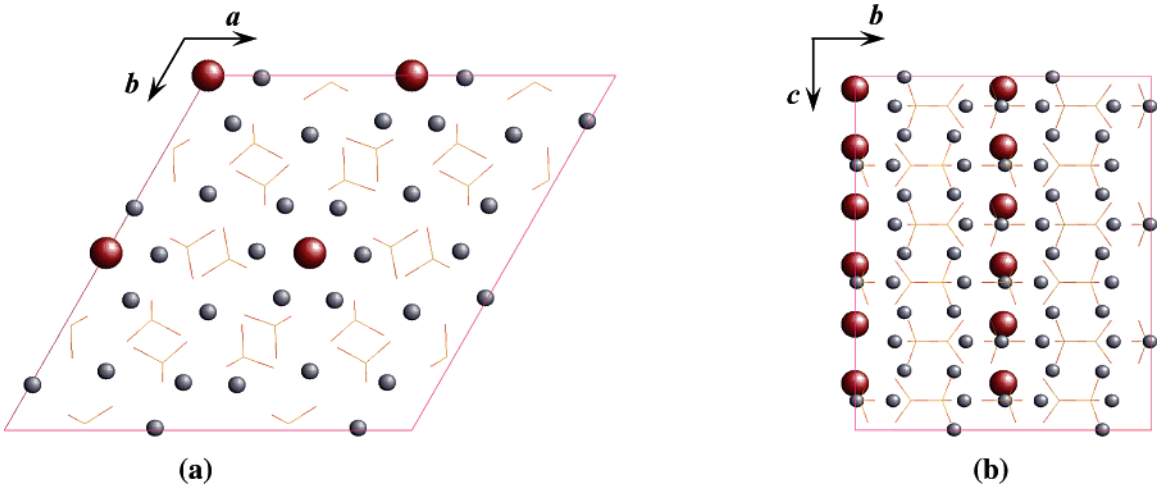

Figure 1. Snapshots of the 2 × 2 × 3 supercell of bromapatite: (a) *ab* plane view, showing evidence of the hexagonal symmetry around the bromide anion and (b) side view along the crystallographic *c*-axis. Ca^{2+} = gray circles, Br^{-} = red circles, PO_4^{3-} = wireframe structure (3D rotable images in *xyz* format are available for hydroxy-, fluor-, chlor-, and bromapatite 2 × 2 × 3 supercells).

TABLE 1: Born−Huggins−Mayer Potential Energy Parameters (Equation 1)

	q_i	A_{ii}/kJ·mol^{-1}	B_{ii}/Å^{-1}	σ_{ii}/Å	C_{ii}/kJ·Å^6·mol^{-1}
Ca	2	11.132	6.250	2.600	8.8928×10^2
P	2.6	20.873	3.333	3.400	2.8139×10^4
O (P)	−1.4	18.786	3.704	2.600	3.1266×10^3
O (H)	−1.6	15.446	4.505	2.600	1.3895×10^3
H	0.6	1.3916	50.000	0.200	1.3552×10^{-3}
F	−1	15.268	2.960	2.358	1.1203×10^3
Cl	−1	15.268	3.087	3.170	7.4384×10^3
Br	−1	15.268	2.980	3.432	1.2407×10^4

Born−Huggins−Mayer (BHM) potential energy function (eq 1, Table 1).

$$U_{ij}(r_{ij}) = \frac{q_i q_j}{r_{ij}} + A_{ij}\exp[B_{ij}(\sigma_{ij} - r_{ij})] - \frac{C_{ij}}{r_{ij}^{6}} \qquad (1)$$

The first term accounts for the Coulombic forces, the exponential term deals with the repulsive interactions arising from the overlap of electronic layers, and the third term represents the van der Waals dispersion energy. Cross parameters were evaluated using the geometrical mean rule. Dipole−quadrupole dispersive interactions (given by an additional $-r_{ij}^{-8}$ term) were not taken into account in the present study; Woodcock et al.[14] have shown that they account for less than 0.5% of the total potential energy, in the alkali halides. The adequacy of the exponential function to describe the repulsive energy term in ionic solids, namely, NaCl-type alkali halides, has been pointed out by several authors.[14−18] Hauptmann et al.[11] proposed a consistent set of parameters for HOAp and FAp based on quantum-chemical calculations and experimental data. They considered the phosphate ions as either rigid or flexible and were able to reproduce the experimental crystal parameters with a maximum error of 1%. Mkhonto et al.[9] developed a similar potential energy function for FAp, and later de Leeuw[10] used the very same potential to study the substitution of the hydroxyl ion for the fluoride ion. In their model, the phosphate P−O bonds were considered to be partly covalent and described by a Morse potential which takes into account bond anharmonicity. In their study of the incorporation of Pu and Cs into the crystal lattice of a substituted fluorapatite (for nuclear waste disposal), Meis et al.[12] modeled the tetrahedral environment of the oxygen ions around phosphorus with a three-body short-range harmonic potential.

For the calcium, phosphate and hydroxyl ions, we worked with the parameters given by Hauptmann and co-workers.[11] Moreover, the phosphate ion was modeled as a rigid tetrahedron, an assumption which proved to give a good account of the physical properties of apatites. All halide ions were modeled using: (i) for the repulsive term, the first set of data of Tosi and Fumi,[16] obtained from crystal data under standard thermodynamic conditions; and (ii) for the dispersive energy, the results of Mayer,[19] based on ultraviolet absorption measurements.

Molecular Geometry and Simulation Details. The positions of all atoms were generated by applying the characteristic symmetry operations for the $P6_3/m$ space group[20] to previously published solid-state X-ray diffraction (XRD) data.[21,22] Simulation boxes were generated by stacking the apatite unit cells in three dimensions as 2 × 2 × 3 or 4 × 4 × 6 supercells, forming a box with a total number of 504 (528 for HOAp) or 4032 (4224 for HOAp) atoms (three-dimensional (3D) rotable images in *xyz* format are available for hydroxy-, fluor-, chlor-, and bromapatite 2 × 2 × 3 supercells). Figure 1 shows a bromapatite supercell. Potential cutoff radii of 8 and 12 Å were used for the 2 × 2 × 3 and 4 × 4 × 6 supercells, respectively. Molecular dynamics simulations were performed using the DL_POLY package.[23] The Verlet algorithm[24,25] was used to integrate the equations of motion; the Ewald summation method[14,25] was employed to calculate the long-range electrostatic interactions; and the Nosé-Hoover anisotropic thermostat-barostat[14,26] was used to control the temperature and/or pressure. It should also be noted that the systems were allowed to relax during 40−60 ps before every calculation. The production runs (160−140 ps) were performed using solids at room temperature (T = 298 K) and atmospheric pressure (p = 1 bar) to calculate the standard molar lattice enthalpy, $\Delta_{lat}H_{298}°$, which was then compared with previously published experimental data, thus checking the accuracy of the runs. The reproducibility and consistency of the calculations were tested by changing the simulation box size, time step, and thermodynamic ensemble: microcanonical (*NVE*), canonical (*NVT*), isothermal−isobaric (*NpT*), and anisotropic isothermal−isobaric (*NσT*). To decrease computer time throughout this study, 2 × 2 × 3 supercells were employed for the high-temperature and high-pressure runs, with a potential cutoff distance of 8 Å and a time step of t = 1 fs. This enabled us to study the apatites under a variety of thermodynamic conditions (T, p), which would otherwise become prohibitively expensive in terms of computer time.

TABLE 2: Crystallographic Data at Room Temperature ($T = 298$ K) and Atmospheric Pressure ($p = 1$ bar) for Hexagonal ($P6_3/m$) Apatites, $\alpha = \beta = 90°$ and $\gamma = 120°$ [a]

	$Ca_{10}(PO_4)_6X_2$											
X	a_{sim}	a_{exp}	δ/%	b_{sim}	b_{exp}	δ/%	c_{sim}	c_{exp}	δ/%	$V_{m,sim}$	$V_{m,exp}$	δ/%
						$2 \times 2 \times 3$ Simulation Box						
OH	9.634	9.418	(+2.3)	9.893	9.416	(+5.0)	6.841	6.875	(−0.5)	564.9	527.8	(+7.0)
F	9.411	9.398	(+0.1)	10.063	9.397	(+7.1)	6.783	6.878	(−1.4)	557.1	526.0	(+6.0)
Cl	10.116	9.598	(+5.4)	10.207	9.598	(+6.3)	6.667	6.776	(−1.6)	584.1	540.6	(+8.0)
Br	10.470	9.761	(+7.3)	9.533	9.761	(−2.3)	6.543	6.739	(−2.9)	572.7	556.1	(+3.0)
						$4 \times 4 \times 6$ Simulation Box						
OH	9.613	9.418	(+2.1)	9.981	9.416	(+6.0)	6.786	6.875	(−1.3)	569.8	527.8	(+8.0)
F	9.257	9.398	(−1.5)	10.072	9.397	(+7.2)	6.755	6.878	(−1.8)	548.8	526.0	(+4.3)
Cl	9.347	9.598	(−2.6)	10.295	9.598	(+7.3)	6.615	6.776	(−2.4)	556.9	540.6	(+3.0)
Br	10.424	9.761	(+6.8)	9.479	9.761	(−2.9)	6.613	6.739	(−1.9)	569.5	556.1	(+2.4)

[a] Cell parameters in Å and molar volume in $Å^3 \cdot mol^{-1}$. Experimental data for HOAp, FAp, and ClAp from ref 21 and from ref 22 in the case of BrAp.

3. Results and Discussion

Room Temperature and Atmospheric Pressure Simulations: Structural Data. The solid structure of the apatites maintained its integrity during the entire simulation run, under the various ensemble conditions (*NVE*, *NVT*, *NpT*, and *NσT*). For the *NσT* ensemble, room temperature ($T = 298$ K) and atmospheric pressure ($p = 1$ bar) results are presented in Table 2.

For the larger supercell, deviations from experimental data of the molar volume have maximum errors of ca. 4% (8% for HOAp). It appears that when the smaller supercells are used, a slight inconsistency is introduced in the calculations, probably due to finite size effects: only in runs with larger simulation boxes do the simulated molar volumes follow the general trend of a regular increase in V_m from FAp to BrAp. This is probably due to the long-range correction algorithms employed in the MD technique to evaluate the energy beyond the potential cutoff. ClAp requires the usage of a larger sample of solid ($4 \times 4 \times 6$ simulation box) to achieve the desired precision in the absolute values of molar volume. In all cases, the accuracy of the simulated lattice angles is generally good, the agreement between calculated and experimental values being within 1.5% and, for most cases, well below this value. In the case of hydroxyapatite, the higher deviation shown for the molar volume is most likely due to a deficient potential parametrization for the hydrogen atom (Hauptmann et al.[11] only studied monoclinic forms, $P2_1/b$). In fact, when applied to hexagonal structures, their potential parameters for the dispersive interaction between hydrogen and the oxygen of phosphate, $C_{O(P)-H}$, led to convergence problems during the simulations. To solve this problem $C_{O(P)-H}$ was set to zero, which should not significantly alter the calculated potential energy. Nevertheless, this parameter inconsistency, found only for the hydroxy ion in the apatite crystals, can explain the larger observed structural deviations. The same deficiency probably accounts for the discrepancy observed when the molar volume of hydroxyapatite is compared with those of fluor- and chlorapatites. The experimental values show that the molar volume of hydroxyapatite is only slightly larger than the corresponding value for fluorapatite and considerably smaller than that of chlorapatite.

Room Temperature and Atmospheric Pressure Simulations: Standard Molar Lattice Enthalpy. The potential energy calculated in the MD runs, excluding the (small) kinetic energy fluctuations, represents a true cohesive energy of the solid. This binding energy corresponds to the internal energy change,[27−30] $\Delta_{lat}U_{298}°$, associated with the following process at 298.15 K

$$Ca_{10}(PO_4)_6X_2(cr) = 10\ Ca^{2+}(g) + 6PO_4^{3-}(g) + 2X^-(g) \quad (2)$$

where X = OH, F, Cl, and Br. Assuming gas-phase ideality for the ions, the corresponding lattice enthalpy can be determined from

$$\Delta_{lat}H_{298}° = \Delta_{lat}U_{298}° + 18RT \quad (3)$$

since the pV term for the crystalline apatite is negligible in comparison with $18RT$ for the gaseous ions. A more detailed discussion of the relationship between lattice energy and lattice enthalpy can be found in a recent paper by Jenkins.[31] The standard molar lattice enthalpies can also be calculated from eq 4

$$\Delta_{lat}H_{298}° = 10\Delta_fH_m°(Ca^{2+}, g) + 6\Delta_fH_m°(PO_4^{3-}, g) + 2\Delta_fH_m(X^-, g) - \Delta_fH_m°[Ca_{10}(PO_4)_6X_2, cr] \quad (4)$$

using $\Delta_fH_m°[Ca_{10}(PO_4)_6(OH)_2, cr] = -13399 \pm 11$ kJ·mol^{-1},[32] $\Delta_fH_m°[Ca_{10}(PO_4)_6F_2, cr] = -13598 \pm 10$ kJ·mol^{-1},[32−34] $\Delta_fH_m°[Ca_{10}(PO_4)_6Cl_2, cr] = -13231 \pm 82$ kJ·mol^{-1},[32] $\Delta_fH_m°[Ca_{10}(PO_4)_6Br_2, cr] = -13063 \pm 81$ kJ·mol^{-1},[32] $\Delta_fH_m°(Ca^{2+}, g) = 1925.9 \pm 0.8$ kJ·mol^{-1},[35] $\Delta_fH_m°(PO_4^{3-}, g) = 302 \pm 22$ kJ·mol^{-1},[36] $\Delta_fH_m°(OH^-, g) = -143.5 \pm 8.0$ kJ·mol^{-1},[35] $\Delta_fH_m°(F^-, g) = -255.39 \pm 0.80$ kJ·mol^{-1},[35] $\Delta_fH_m°(Cl^-, g) = -233.13 \pm 0.80$ kJ·mol^{-1},[35] $\Delta_fH_m°(Br^-, g) = -219.07 \pm 0\ 0.80$ kJ·mol^{-1}.[35]

The experimental values thus obtained are compared in Table 3 with the corresponding lattice enthalpies derived from the simulation results through eq 3. The uncertainties quoted, associated with experimental data, are estimated to be twice the standard deviation (2σ) of the statistical mean. Also included

TABLE 3: Lattice Enthalpies of the Apatites at $T = 298$ K and $p = 1$ bar

	$\Delta_{lat}H_{298}°[Ca_{10}(PO_4)_6X_2]$/kJ·mol^{-1}						
X	exptl[a]	simulation[b]	δ/%	simulation[c]	δ/%	eq 5	δ/%
OH	34183 ± 134	34044	(−0.4)	34129	(−0.2)	32953	(−3.6)
F	34158 ± 133	33662	(−1.5)	33522	(−1.9)	33191	(−2.8)
Cl	33836 ± 156	33354	(−1.4)	33237	(−1.8)	32783	(−3.1)
Br	33696 ± 155	33211	(−1.4)	33192	(−1.5)	32633	(−3.2)

[a] Experimental values derived from eq 4 (see text). [b] Calculated from eq 3 using MD simulation runs with $4 \times 4 \times 6$ simulation boxes. [c] Calculated from eq 3 using MD simulation runs with $2 \times 2 \times 3$ simulation boxes.

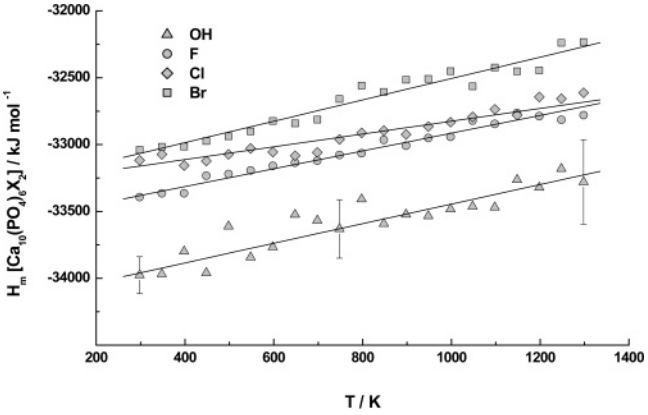

Figure 2. Correlation plots of the molar enthalpy as a function of absolute temperature ($p = 1$ bar).

in Table 3 are the lattice enthalpies calculated from eq 5,[37−38]

$$\Delta_{\mathrm{lat}}U_{298}^{\circ} = AI\left(\frac{2I}{V_{\mathrm{m}}}\right)^{1/3} \tag{5}$$

where $A = 121.39$ kJ·mol^{-1}, I is the lattice ionic strength, and V_{m} is the volume of the molecular formula unit. In the present case, $I = (1/2)[10 \times 2^2 + 6(-3)^2 + 2(-1)^2] = 48$ and $V_{\mathrm{m}} = V_{\mathrm{cell}}/Z$, where V_{cell} is the unit cell volume and Z is the number of formula units per unit cell ($Z = 1$ for the $Ca_{10}(PO_4)_6X_2$ formula unit). Recently, Kim and co-workers[39] obtained very accurate values for the molar volumes of calcium and lead apatites, using synchrotron X-ray radiation and neutron diffraction techniques. Predictions from eq 5 are based on the following unit cell volumes for the hexagonal phases of the apatites: $V_{\mathrm{cell}}[Ca_{10}(PO_4)_6(OH)_2] = 530.7$ Å^3,[39] $V_{\mathrm{cell}}[Ca_{10}(PO_4)_6F_2] = 519.4$ Å^3,[39] $V_{\mathrm{cell}}[Ca_{10}(PO_4)_6Cl_2] = 539.0$ Å^3,[39] $V_{\mathrm{cell}}[Ca_{10}(PO_4)_6Br_2] = 546.5$ Å^3.[39] From Table 3 it can be seen that the molecular simulations reproduce the experimental lattice enthalpy values to better than 2%. Somewhat higher deviations are obtained using eq 5. These deviations are, however, considerably smaller than the 7% accuracy limit obtained from application of eq 5 to a very large number of compounds.[37]

The results of Table 3 show that the BHM potential energy function adequately describes the energetics of the apatites' crystal structure, reproducing the experimental values to ca. 2%. Potential energies and lattice enthalpies do not significantly vary when the simulation box size increases from $2 \times 2 \times 3$ to $4 \times 4 \times 6$.

High-Temperature Simulations: Heat Capacity at Constant Pressure. To investigate the thermal properties of the apatites, molecular dynamics runs were performed at $p = 1$ bar and spanning a temperature range from 298 to 1298 K. The variation of the standard molar enthalpy (H_{m}) with temperature, at 50 K intervals, is plotted in Figure 2. The scatter increases with temperature but, for the sake of simplicity, error bars are only represented for hydroxyapatite at a few chosen temperatures. It should be noted that the error bars indicated in Figure 2, for HOAp, correspond to uncertainties of 0.4% and 1.6% in the low- and high-temperature regions, respectively. For the other apatites, the statistical standard deviation of the $H_{\mathrm{m}}-T$ data is always less than 1%.

The molar enthalpy is satisfactorily described by a linear correlation—eq 6—leading to an average value for $C_{p,\mathrm{m}} = (\partial H_{\mathrm{m}}/\partial T)_p$, over the whole temperature range. However, in the case of chlorapatite the results appear to show a slight decrease in the slope in the range 580−780 K.

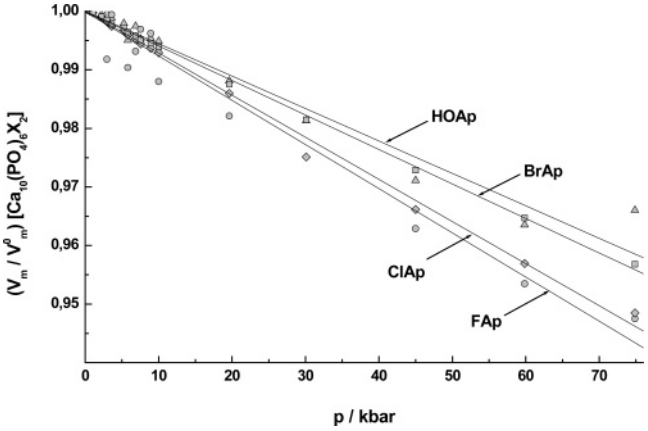

Figure 3. Isothermal lines of normalized volume as a function of pressure ($T = 298$ K).

TABLE 4: Correlation Parameters of the Molar Enthalpy as a Function of Temperature (Equation 6)

	$Ca_{10}(PO_4)_6X_2$		
X	$H_{\mathrm{m},298}$/kJ·mol^{-1}	$C_{p,\mathrm{m}}$/J·mol^{-1}·K^{-1}	R^2
OH	−34133 ± 58	694 ± 68	0.85
F	−33563 ± 22	646 ± 26	0.97
Cl	−33339 ± 29	530 ± 34	0.93
Br	−33314 ± 36	811 ± 42	0.95

$$H_{\mathrm{m}} = (H_{\mathrm{m},298} - 298C_{p,\mathrm{m}}) + C_{p,\mathrm{m}}T \tag{6}$$

The correlation parameters are listed in Table 4. $H_{\mathrm{m},298}$ should be the enthalpy value at 298 K and indeed the values recorded in Table 4 agree within 0.2% with the MD results (not shown). There are some experimental values for the heat capacities at constant pressure of the apatites. Egan et al.[40] used a calorimetric technique to determine $C_{p,\mathrm{m}}$ for hydroxyapatite, obtaining a value of $C_{p,\mathrm{m}} = 769$ J·mol^{-1}·K^{-1} at 298 K, in agreement with the MD result within 10%. For fluorapatite, Meis et al.[12] measured a value of $C_{p,\mathrm{m}} = 740$ J·mol^{-1}·K^{-1} at 300 K by differential calorimetry; this value differs by about 13% from the MD simulations result.

High-Pressure Simulations: Isothermal Compressibility. High-pressure calculations were carried out at room temperature ($T = 298$ K) in the range 0.5−75 kbar, under the *NσT* anisotropic isothermal−isobaric ensemble, which allows the solid structure to deform freely in space, without imposing an "artificial" isotropic deformation to the crystal. The description of the molar volume, as pressure is applied at constant temperature, leads to the isothermal compressibility, $\kappa_{\mathrm{T}} = -(1/V)(\partial V/\partial p)_T$. To obtain a better insight into the behavior of compressed apatites, the molar volume was normalized by dividing it by the zero pressure value (eq 7). In the case of hydroxyapatite, this has the added advantage of minimizing the effects of the deficiencies in the potential, discussed in the Structural Data section. The reduced values are plotted against the corresponding pressure in Figure 3. In the studied pressure range the results are well correlated by a linear function; the slopes of the lines (related to the isothermal compressibility) are presented in Table 5, along with the correlation coefficients (R^2).

$$\frac{V_{\mathrm{m}}}{V_{\mathrm{m}}^{\circ}} = 1 - \left[\frac{\partial\left(\frac{V_{\mathrm{m}}}{V_{\mathrm{m}}^{\circ}}\right)}{\partial p}\right]_T p \tag{7}$$

TABLE 5: Correlation Parameters for the Normalized Volume as a Function of Pressure (Equation 7)

	$Ca_{10}(PO4)_6X_2$	
X	$-[\partial(V_m/V_m°)/\partial p]_T$/Å^3·kbar^{-1}·mol^{-1}	R^2
OH	5.5371×10^{-4}	0.98
F	7.5239×10^{-4}	0.96
Cl	7.1972×10^{-4}	1.00
Br	5.9010×10^{-4}	1.00

Murayama et al.[41] found that both HOAp and FAp are stable up to pressures of at least 100 kbar. This excludes the possibility of the value obtained for HOAp at $p = 75$ kbar indicating decomposition of the solid and/or the beginning of any structural change in the crystal lattice. A further simulation at $p = 90$ kbar (not shown) confirmed the general trend for HOAp, thus indicating that the result at 75 kbar is spurious. The compressibilities of HOAp and BrAp, as well as those of FAp and ClAp, are essentially constant and of the same magnitude throughout the entire pressure range. (This can be easily seen from the values of the slope, indicated in Table 5.) In what concerns the compressibility of the apatites, the following order applies: HOAp ≤ BrAp < ClAp ≤ FAp. The position of the hydroxyapatite line relative to that of chlorapatite does not agree with reported data by Brunet et al.,[42] but their samples were of dubious purity. It is well-known[32] that the preparation of hydroxyapatite under open air conditions can lead to carbonate incorporation. Although Brunet confirmed the absence of the carbonate characteristic IR absorption bands at 1400−1600 cm^{-1}, the other characteristic absorption peak[43−45] around 865 cm^{-1} was not investigated. Moreover, Brunet et al. admitted that their samples of fluor- and chlorapatite were contaminated with OH^- (up to about 30% of hydroxyl ions in the case of ClAp!).

Whereas hydroxyapatite is the least compressible of all the apatites, FAp is always the most compressible, probably because of (i) the relatively small ionic radius of the fluoride ion and (ii) its exact location in the center of the triangles formed by the three calcium ions. This structure seems to confer on FAp a greater ability to adapt to external pressure. The intermediate behavior of bromapatite between its chlor- and hydroxy-analogues had not been previously observed.

To throw some light onto this unexpected feature, the total cell volume, V_m, was decomposed into the three contributions along the unit cell lengths, normalized by the usual procedure of division by the corresponding zero pressure values, a_0, b_0, and c_0. The resulting deformation plots are presented in Figure 4. A global analysis seems to indicate that both HOAp and ClAp are most compressible along the *a*-axis and least compressible along the *b*-axis. As for BrAp, the least compressible direction is that of the *c*-axis, with both the *a* and *b* axes responding similarly to pressure. It can be seen from Figure 4 that hydroxy- and chlorapatite are similar in their response to pressure along the *a* and *b* crystallographic axes. It should be recalled that these axes characterize the planes defined by the three Ca^{2+} ions, whereas the *c*-axis is associated with the position of the X species. The latter is the more interesting from the elastic deformation point of view, for it appears that the bigger bromide ion (relative to either the hydroxyl or chloride ions) precludes the *c*-axis being the most favorable direction for deformation in the case of BrAp. The different responses (to pressure) of the crystal along the three crystallographic axes confirm the anisotropic cell compression, previously predicted by Brunet et al.[42] for HOAp and ClAp, and by Matsukage et al.[46] for a natural apatite sample, $[Ca_{10}(PO_4)_6F_{1.88}Cl_{0.12}]$.

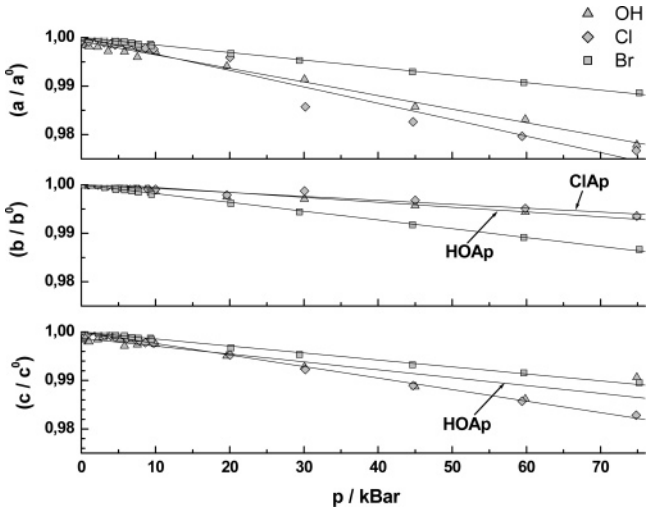

Figure 4. Deformation plots of the normalized unit cell lengths as a function of pressure ($T = 298$ K).

Isothermal Equation of State. It is well-known that the Tait equation of state (eq 8), developed for compressed liquids,[47] can be successfully applied to many inorganic solids under pressure.[48] However, its semiempirical character makes it less suitable for the description of a full set of results, like ours, covering a wide pressure range. In what concerns the apatites, we have confirmed that the linear dependence on pressure predicted by eq 8 can only be retrieved for $p > 10$ kbar.

$$\frac{V_0 p}{V - V_0} = ap + b \tag{8}$$

The behavior of apatites under compression has also been studied by Brunet et al.[42] and Matsukage et al.[46] They used an equation of state derived by Birch,[49] based on a treatment of the finite deformation of elastic solids due to Murnaghan.[50] The pressure is now explicitly given as a function of the so-called Eulerian finite strain, $[(V_0/V)^{2/3} - 1]/2$. Although the resulting equation (BM-EoS) can be used in its second- and third-order forms,[51] both Matsukage et al. and Brunet et al. were able to fit their high-pressure data to the second-order form. In the present case it was found that even the third-order form would not adequately represent our MD data.

A more theoretically based approach has been developed by Vinet and co-workers,[52] aiming at a universal equation for solids. The various classes of solids—rare-gas, ionic, covalent, and metallic—can be distinguished by their rather different types of atomic interactions. While it has been recognized that the repulsive part of the potential plays a major role in determining the structure of the condensed phases, ionic and van der Waals interactions, which fall off more slowly with distance than overlap interactions, cannot be neglected in ionic compounds, such as apatites. However, under compression, overlap effects are significant for all classes of solids. On the basis of this, Vinet et al.[52] were able to arrive at a three-parameter universal equation of state for all classes of solids under compression. The three parameters are the zero-pressure values of (i) the molar volume, V_0, (ii) the isothermal bulk modulus, $B_0 = -V(\partial p/\partial V)_T$, and (iii) the pressure derivative of the bulk modulus, $(\partial B/\partial p)_0$. Parsafar and Mason[53] improved on the work of Vinet and co-workers, and derived an equation which is both simpler and more accurate for a wide variety of substances, including some which undergo phase transitions. Stressing that for solids under strong compression only the rather featureless repulsive branch

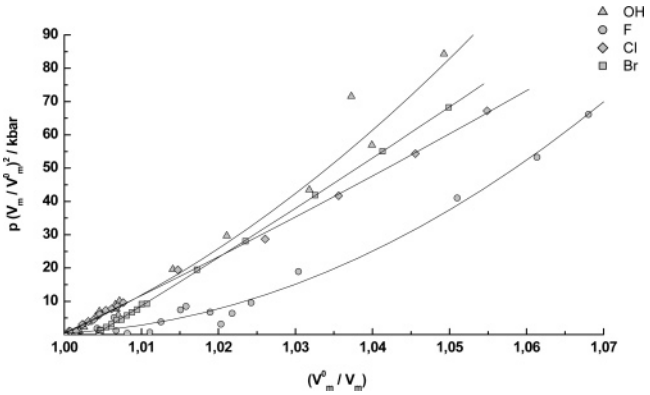

Figure 5. MD results and correlation plots using the PM-EoS (T = 298 K).

TABLE 6: Parameters of the PM-EoS (Equation 9) and Correlation Coefficients

	$Ca_{10}(PO4)_6X_2$			
X	A_0/kbar	A_1/kbar	A_2/kbar	R^2
OH	1.1461×10^4	-2.3949×10^4	1.2487×10^4	0.99
F	1.1940×10^4	-2.4038×10^4	1.2099×10^4	0.99
Cl	6.1763×10^2	-2.3444×10^3	1.7272×10^3	1.00
Br	-3.0717×10^1	-1.3615×10^3	1.3866×10^3	1.00

of the binding-energy curve matters, they were able to show that pV^2 should be a quadratic function of the density, $\rho = 1/V$ (eq 9).

$$p\left(\frac{V}{V^o}\right)^2 = A_0 + A_1\left(\frac{V^o}{V}\right) + A_2\left(\frac{V^o}{V}\right)^2 \qquad (9)$$

A_0, A_1, and A_2 are simple functions of the molar volume, bulk modulus, and its pressure derivative (all at zero pressure)—the three parameters of the original equation developed by Vinet et al. The Parsafar and Mason equation of state (abbreviated PM-EoS), eq 9, gives the correct asymptotic limit, predicting $V = 0$ at infinite pressure (unlike Tait's equation, which predicts a finite, negative value). Equation 9 has proven extremely useful in describing the high-pressure behavior not only of ionic compounds (LiF, NaCl, CsI, Fe_3O_4, $MnSnO_3$, etc) but also of noble-gas (Ar) and polar-gas (NH_3) solids, quantum solids (He, Ne, H_2), metals (Cu, Ce), and hydrocarbons (n-C_8H_{18}, n-$C_{16}H_{34}$, acenaphtene). It seemed thus worthwhile to apply the PM-EoS to our high-pressure MD experiments. As expected, the isotherms are well described by the PM-EoS in the whole pressure range, including the low-pressure end, Figure 5 (the HOAp value at $p = 75$ kbar was excluded from the correlation). The values of the polynomial constants, A_0, A_1, and A_2, and of the corresponding correlation coefficients are recorded in Table 6.

The goodness of the correlation means that the deviation between the predicted molar volumes and the corresponding MD results is less than 1%, the exception being the molar volume of FAp at 0.5 kbar which is 2.5% higher than the simulated value.

4. Conclusions

The structural model and potential energy function employed in the simulations of the apatites have been validated by the agreement, within 2%, of the values for the lattice enthalpy obtained from reaction−solution calorimetry[32] and from molecular dynamics studies (Table 3). Although the rigid phosphate structure neglects covalent-bonded atomic interactions, it proves to be a suitable approximation for the description of atomic interactions and (hexagonal) crystal structure of the apatites. A similar conclusion had been reached by Hauptmann et al.[11] for both monoclinic HOAp and hexagonal FAp, after modeling the phosphate ion as either a rigid or a flexible tetrahedron.

The isothermal line of the normalized volume ($V_m/V_m°$) for bromapatite is located between those for chlorapatite and hydroxyapatite. This intermediate behavior was further investigated by plotting the normalized unit cell lengths (Figure 4) for the three compounds, as function of pressure. It then became clear that, whereas HOAp and ClAp are most compressible along the crystallographic *a*-axis and least compressible along the *b*-axis, in the case of BrAp the *b*-axis becomes the most compressible direction and *c* the least compressible one. The deformation of the apatites is elastically anisotropic in all cases. It should be noted that neither chlorapatite nor bromapatite have ever been the subject of MD simulations.

The $p-V_m$ data in the range 1−75 kbar are well described by the PM-EoS in its three-parameter, second-order polynomial form. This equation will, no doubt, prove very useful in future studies involving apatites: (i) in the low/medium-pressure range, to model the behavior of apatites in the solar system,[54] and (ii) at high pressures, to control hydroxyapatite processing in the biomaterials industry.[7,55] In what concerns bone, since carbonated hydroxyapatite is its major inorganic component, the PM-EoS could also be used to predict its structural−mechanical properties.[56] Geochemical studies involving solid solutions of apatites in the Earth's upper mantle[3] (200 K < T < 1770 K) will also require the knowledge of the temperature dependence of the parameters of the PM-EoS. These calculations will be carried out in future work, using the approximations suggested by the equation's originators:[53] (i) the standard molar heat capacity at constant volume (C_v) is independent of temperature, and (ii) the calculations should be restricted to $T > \Theta_D$, where Θ_D is the Debye characteristic temperature. The study of the monoclinic ($P2_1/b$) phases of hydroxy- and chlorapatite is now under way and will be reported soon.

Acknowledgment. The authors thank Professor H. D. B. Jenkins (Warwick University, Coventry, U.K.), for helpful comments. F. J. A. L. Cruz gratefully acknowledges a PhD grant from *Fundação para a Ciência e a Tecnologia* (FCT/SFRH/3077/2000).

Supporting Information Available: Data files (.cif) of $Ca_{10}(PO_4)_6(X)_2$ (X = OH, F, Cl, Br). This material is available free of charge via the Internet at http://pubs.acs.org.

References and Notes

(1) Greenwood, N. N.; Earnshaw, A. *Chemistry of the Elements*, 2nd ed.; Butterworth-Heinemann: Oxford and Boston, 1997.

(2) Fegley, B., Jr. *Icarus* **1980**, *41*, 439.

(3) Lodders, K.; Fegley, B., Jr. *The Planetary Scientist's Companion*; Oxford University Press: Oxford, 1998.

(4) Lodders, K. *Astrophys. J.* **2003**, *591*, 1220.

(5) Peters, F.; Epple, M. *Z. Kardiol.* **2001**, *90*: Suppl.3, III81.

(6) Dorozhkin, S. V.; Epple, M. *Angew. Chem., Int. Ed.* **2002**, *41*, 3130.

(7) Tadic, D.; Peters, F.; Epple, M. *Biomaterials* **2002**, *23*, 2553.

(8) Vallet-Regí, M. *J. Chem. Soc., Dalton Trans.* **2001**, *2*, 97.

(9) Mkhonto, D.; de Leeuw, N. H. *J. Mater. Chem.* **2002**, *12*, 2633.

(10) de Leeuw, N. H. *Phys. Chem. Chem. Phys.* **2004**, *6*, 1860.

(11) Hauptmann, S.; Dufner, H.; Brickmann, J.; Kast, S.; Berry, R. S. *Phys. Chem. Chem. Phys.* **2003**, *5*, 635.

(12) Meis, C.; Gale, J. D.; Boyer, L.; Carpena, J.; Gosset, D. *J. Phys. Chem. A* **2000**, *104*, 5380.

(13) Born, M.; Huang, K. *Dynamical Theory of Crystal Lattices*; Oxford University Press: Oxford, 1988.

(14) Woodcock, L. V.; Singer, K. *Trans. Faraday Soc.* **1971**, *67*, 12. Woodcock, L. V. *J. Chem. Soc., Faraday Trans. 2* **1974**, *70*, 1405. Lewis, J. W. E.; Singer, K.; Woodcock, L. V. *J. Chem. Soc., Faraday Trans. 2* **1975**, *71*, 301.

(15) Tosi, M. P. *J. Phys. Chem. Solids* **1963**, *24*, 965.

(16) Tosi, M. P.; Fumi, F. G. *J. Phys. Chem. Solids* **1964**, *25*, 31. Tosi, M. P.; Fumi, F. G. *J. Phys. Chem. Solids* **1964**, *25*, 45.

(17) Pettitt, B. M.; Rossky, P. J. *J. Chem. Phys.* **1986**, *84*, 5836.

(18) Huggins, M. L.; Mayer, J. E. *J. Chem. Phys.* **1933**, 1, 643.

(19) Mayer, J. E. *J. Chem. Phys.* **1933**, *1*, 270.

(20) *International Tables for Crystallography*; Hahn, T., Ed.; Reidel Publishing Company: Dordrecht, 1983.

(21) Hughes, J. M.; Cameron, M.; Crowley, K. D. *Am. Mineral.* **1989**, *74*, 870.

(22) Elliott, J. C.; Dykes, E.; Mackie, P. E. *Acta Crystallogr., B* **1981**, *B37*, 435.

(23) Smith, W.; Forrester, T. R. *The DL_POLY package of molecular simulation routines, version 2.12*; The Council for the Central Laboratory of Research Councils: Daresbury Laboratory, Warrington, U.K., 1999.

(24) Verlet, L. *Phys. Rev.* **1967**, *159*, 98.

(25) van Gunsteren, W. F.; Berendsen, H. J. C. *Angew. Chem., Int. Ed. Engl.* **1990**, *29*, 992.

(26) Nosé, S. *J. Chem. Phys.* **1984**, *81*, 511.

(27) Greenwood, N. N. *Ionic Crystals, Lattice Defects and Nonstoichiometry*; Butterworth: London, 1970.

(28) Johnson, D. A. *Some Thermodynamic Aspects of Inorganic Chemistry*, 2nd ed.; Cambridge University Press: Cambridge, 1982.

(29) Dasent, W. E. *Inorganic Energetics*, 2nd ed.; Cambridge University Press: Cambridge, 1982.

(30) West, A. R. *Basic Solid State Chemistry*, 2nd ed.; John Wiley: Chichester, 1999.

(31) Jenkins, H. D. B. *J. Chem. Educ.* **2005**, *82*, 950.

(32) Cruz, F. J. A. L.; Minas da Piedade, M. E.; Calado J. C. G. *J. Chem. Thermodyn.* **2005**, *37*, 1061.

(33) Ben Cherifa, A.; Somrani, S.; Jemal, M. *J. Chim. Phys.* **1991**, *88*, 1893.

(34) Jemal, M.; Ben Cherifa, A.; Khattech, I.; Ntahomvukiye, I. *Thermochim. Acta* **1995**, *259*, 13.

(35) Wagman, D. D.; Evans, W. H.; Parker, V. B.; Schumm, R. H.; Halow, I.; Bailey, S. M.; Churney, K. L.; Nuttall, R. L. The NBS Tables of Chemical Thermodynamic Properties. *J. Phys. Chem. Ref. Data* **1982**, *11*, Supplement no. 2.

(36) The value $\Delta_f H_m°(PO_4^{3-}, g) = (302 \pm 22)$ kJ·mol^{-1} was obtained from $\Delta_f H_m°(PO_4^{3-}, g) = \Delta_f H_m°(PO_4^{3-}, ao) - \Delta_f H_m°(PO_4^{3-}) - 3[\Delta_f H_m°(H^+, g) + \Delta_{hyd} H_m°(H^+)]$, by using $\Delta_f H_m°(H^+, g) = 1536.202 \pm 0.080$ kJ·mol^{-1} and $\Delta_f H_m°(PO_4^{3-}, ao) = -(1277.4 \pm 8.0)$ kJ·mol^{-1} given in ref 37 and $\Delta_{hyd} H_m°(H^+) = -1103 \pm 7$ kJ·mol^{-1} and $\Delta_{hyd} H_m°(PO_4^{3-}) = -2879$ kJ·mol^{-1} proposed in: Marcus, Y. *J. Chem. Soc., Faraday Trans.* **1987**, *83*, 339.

(37) Glasser, L.; Jenkins, H. D. B. *J. Am. Chem. Soc.* **2000**, *122*, 632.

(38) Flora, N. J.; Yoder, C. H.; Jenkins, H. D. B. *Inorg. Chem.* **2004**, *43*, 2340.

(39) Kim, J. Y.; Fenton, R. R.; Hunter, B. A.; Kennedy, B. J. *Aust. J. Chem.* **2000**, *53*, 679.

(40) Egan, E. P.; Wakefield, Z. T.; Elmore, K. L. *J. Am. Chem. Soc.* **1950**, *72*, 2418.

(41) Murayama, J. K.; Makai, S.; Kato, M.; Kumazawa, M. *Phys. Earth Planet. Inter.* **1986**, *44*, 293.

(42) Brunet, F.; Allan, D. R.; Redfern, S. A. T.; Angel, R. J.; Miletich, R.; Reichmann, H. J.; Sergent, J.; Hanfland, M. *Eur. J. Mineral.* **1999**, *11*, 1023.

(43) Ben Cherifa, A.; Khattech, I.; Jemal, M. *Ann. Chim. Fr.* **1988**, *13*, 57.

(44) Wilson, R. M.; Elliott, J. C.; Dowker, S. E. P. *J. Solid State Chem.* **2003**, *174*, 132.

(45) LeGeros, R. Z. *Hydroxyapatite and related materials*; CRC Press: Boca Raton, FL, 1994.

(46) Matsukage, K. N.; Ono, S.; Kawamoto, T.; Kikegawa, T. *Phys. Chem. Miner.* **2004**, *31*, 580.

(47) Rowlinson, J. S.; Swinton, F. L. *Liquids and liquid mixtures*; Butterworth: London, 1982.

(48) Couchman, P. R.; Reynolds, C. L. *J. Appl. Phys.* **1976**, *47*, 5201.

(49) Birch, F. *Phys. Rev.* **1947**, *71*, 809.

(50) Murnaghan, F. D. *Am. J. Math.* **1937**, *49*, 235.

(51) Angel, R. J. *Rev. Mineral. Geochem.* **2000**, *41*, 35.

(52) Vinet, P.; Ferrante, J.; Smith, J. R.; Rose, J. H. *J. Phys. C* **1986**, *19*, L467.

(53) Parsafar, G.; Mason, E. A. *Phys. Rev. B* **1994**, *49*, 3049.

(54) Pollack, J. B.; Yung, Y. L. *Annu. Rev. Earth Planet. Sci.* **1980**, *8*, 425.

(55) Rodriguez-Lorenzo, L. M.; Vallet-Regí, M.; Ferreira, J. M. F. *Biomaterials* **2001**, *22*, 583.

(56) Weiner, S.; Wagner, H. D. *Annu. Rev. Mater. Sci.* **1998**, *28*, 271.